Recent Res. Devel. Fluid Dynamics, 3 (2000):113-123 ISBN : 81 - 86846 - 86 - 7

Strong shock waves in a dense gas

José M. Montanero[1] and Vicente Garzó[2]
[1]Departamento de Electrónica e Ingeniería Electromecánica, Universidad de Extremadura, E-06071 Badajoz, Spain; [2]Departamento de Física, Universidad de Extremadura, E-06071, Badajoz, Spain

ABSTRACT

An overview of recent work on plane shock waves in a hard-sphere fluid is presented. The analysis is made within the framework of the Enskog theory and three different and complementary routes are used:(i) the standard hydrodynamic approaches at the levels of Navier-Stokes and (linear) Burnett orders but considering the expressions of the transport coefficients derived from the Enskog equation; (ii) the use of Holian's hypothesis which takes the Navier-Stokes relations but modifying the thermal dependence of the transport coefficients; and (iii) the solution of the full Enskog equation by means of the direct simulation Monte Carlo method. A comparison between the profiles of the hydrodynamic fields and dissipative fluxes obtained from the different approaches is carried out for several values of density and Mach number. The results indicate that the theoretical predictions underestimate the shock thickness. This effect becomes more important at low densities and high Mach numbers. In general, the Holian theory agrees much better with Monte Carlo simulations than the Navier-Stokes and (linear) Burnett approximations,

Transworld
Research Network
T.C. 36/248(1),
Trivandrum-695 008, India.

in contrast to the well-known superiority of the Burnett theory for dilute gases.

1 INTRODUCTION

Needless to say, normal shock waves is one of the most interesting problems in fluid dynamics. They provide a convenient way of determining thermodynamic data under extreme conditions. These waves occupy a small, rapidly moving transition region in space connecting two equilibrium states, namely, a relatively cold, low-pressure region and a relative hot, high-pressure region [1]. Strong shock waves appear in many and different physical phenomena where their common characteristic is the abrupt spatial change of the hydrodynamic fields over a (macroscopic) short distance. Because of the extremely sharp gradients in the hydrodynamic fields, the search for accurate theories to fully describe the shock profiles is still an open problem. As a matter of fact, it is well-known that the Navier-Stokes (NS) equations do not accurately describe the shock profiles under conditions of low-density hypersonic flows [2, 3, 4, 5, 6]. This inconvenient has motivated the use of alternative theoretical approaches. In the context of the continuum description, the Burnett theory [4, 5, 6] and a modified NS approach [7] give an improvement over the standard NS predictions as compared with simulations. Other different approaches carried out are the bimodal distribution of Mott-Smith [8] and the Grad's moment method [9]. All these theories have been complemented by computer simulations, both using molecular dynamics [6, 10, 11] and Monte Carlo methods [12]. In absence of experimental data, the numerical results obtained via microscopic simulations must be considered as the only way to check and determine the range of validity of the different theoretical approaches.

In the case of a dilute gas, the Chapman-Enskog expansion of the Boltzmann equation provides explicit formulas of the transport coefficients both in the NS and Burnett approximations [13]. As said before, under conditions of hypersonic flows, Fiscko and Chapman [2] and Salomons and Mareschal [6] have shown that the Burnett predictions are significantly more accurate than that of the NS. This conclusion was obtained by comparing the theoretical shock profiles with the numerical results obtained from Monte Carlo and molecular dynamics simulations. On the other hand, since the NS equations provide a reasonable description of the shock profiles and preserve a much simpler mathematical structure, Holian [7] introduced a slight modification to the NS equations. In this modification, designated as Holian's conjecture, the temperature dependence of the NS transport coefficients is through the component of the temperature T_{xx} in the direction of the shock wave propagation instead of the average temperature T. The theory of Holian leads to a substantial improvement of the agreement with simulation data over the standard NS equations [14]. Nevertheless, recently Uribe *et al.* [15] have given evidence of the superiority of the Burnett approach over the NS and Holian theories.

In the context of dense fluids, pioneering papers [10, 11] using molecular dynamics simulations for a Lennard-Jones fluid showed that the discrepancies between simulation data and the NS predictions were very small. An interesting question is whether, as occurs in a dilute gas, the NS predictions for the shock profiles are qualitatively improved when the Burnett corrections are taken into account. One of the main difficulties in extending the continuum approach beyond the low-density limit is that, in general, the density dependence of the transport coefficients is not explicitly known. Nevertheless, a notable exception is the hard-sphere model, for which the Enskog theory [16] represents an adequate description over a wide range of length and time scales. In this framework, the transport coefficients have been calculated up to the linearized Burnett hydrodynamic order [17, 18], and the corresponding density, velocity, and temperature profiles have been numerically computed for different values of both the Mach number and the reduced density [19]. In order to determine the accuracy of the different approaches, the NS and Burnett predictions have been compared with simulation data obtained from a recently proposed simulation Monte Carlo method [20]. The results [21] indicate that the NS theory leads to a description of plane shock waves better for dense gases than for dilute gases, thus confirming previous observations for other potentials [10, 11]. Surprisingly, the NS predictions are even better than those of the (linear) Burnett theory at moderate densities and high Mach numbers. This last result motivated to Montanero *et al.* [22] to extend the Holian's recipe to the finite density regime. The comparison shows that Holian's recipe exhibits the best overall performance over the remaining approaches.

In this review, we present a survey of recent work on strong shock waves in a hard-sphere fluid described by the Enskog equation. The organization of the review is as follows. In Sec. II, we expose the standard hydrodynamic approaches at the levels of the NS and Burnett orders but considering the expressions of the transport coefficients derived from the standard and revised Enskog theory. The use of Holian's hypothesis is extended for a dense hard-sphere fluid in Sec. III. In Sec. IV, we briefly describe the direct Monte Carlo simulation method as applied to the plane shock wave problem. In Sec. V, we present the results for the profiles of the hydrodynamic fields, dissipative fluxes, and the shock thickness obtained from the different continuum approaches and from the simulation algorithm. This study is carried out for several values of density and Mach number. The paper is closed in Sec. VI with some concluding remarks.

2 HYDRODYNAMIC DESCRIPTION OF PLANE SHOCK WAVES

2.1 Balance equations

In order to describe the (one-dimensional) hydrodynamic profiles of a plane shock wave, it is convenient to choose a reference frame moving with the shock front, so that the shock is stationary in this frame. Consequently, taking the x axis as the shock wave direction, the hydrodynamic balance equations read

$$\rho(x)u(x) = \text{const}\,, \tag{1}$$

$$P_{xx}(x) + \rho(x)u^2(x) = \text{const}\,, \tag{2}$$

$$\rho(x)u(x)[e(x)+\tfrac{1}{2}u^2(x)] + P_{xx}(x)u(x) + q(x) = \text{const}\,, \tag{3}$$

where ρ is the mass density, u is the x component of the flow velocity, P_{xx} is the xx normal component of the pressure tensor, e is the internal energy per mass unit, and q is the x component of the heat flux. Asymptotically far from the shock front, the fluid is at equilibrium, so that $q = 0$ and $P_{xx} = p$, where p is the hydrostatic pressure. Labeling the unshocked "cold" equilibrium state (upstream) by the subscript 0 and the shocked "hot" equilibrium state (downstream) by the subscript 1, Eqs. (1)–(3) lead to the well-known Rankine-Huginot relations [1]:

$$\rho_0 u_0 = \rho_1 u_1\,, \tag{4}$$

$$p_0 + \rho_0 u_0^2 = p_1 + \rho_1 u_1^2\,, \tag{5}$$

$$\rho_0 u_0(e_0 + \tfrac{1}{2}u_0^2) + p_0 u_0 = \rho_1 u_1(e_1 + \tfrac{1}{2}u_1^2) + p_1 u_1\,. \tag{6}$$

The set of equations (1)–(3) [or (4)–(6)] are a consequence of the conservation of mass, momentum and energy, respectively, so that they apply for any fluid system. In what follows, we will consider the hard-sphere model in the context of the Enskog theory and will use the corresponding explicit expressions for the transport coefficients.

2.2 Application to a dense hard-sphere fluid

Let us consider now the hard-sphere fluid. For a dense hard-sphere gas there is no potential contribution to the internal energy, so that e is simply proportional to the temperature T. More precisely,

$$e = \frac{3k_BT}{2m}\,, \tag{7}$$

where k_B and m are, respectively, the Boltzmann constant and the mass of a particle. The equation of state is

$$p = \frac{\rho k_B T}{m}[1 + 4\eta\chi(\eta)]\,, \tag{8}$$

where $\eta \equiv \pi\rho\sigma^3/6m$ is the packing fraction, σ being the sphere diameter, and $\chi(\eta)$ is the equilibrium value of the pair of correlation function at the point of contact. Here, we will use the Carnahan-Starling approximation [23] for the density dependence of χ, i.e., $\chi(\eta) = (1-\eta/2)/(1-\eta)^3$.

To close the problem, we need to specify the relationship between the fluxes and the hydrodynamic gradients. Obviously, this is a crucial point in the hydrodynamic description of any kind of problem. To linear Burnett order and for the particular geometry of the plane shock wave problem, the constitutive equations can be written as

$$\begin{aligned} P_{xx}(x) &= p(x) - [\tfrac{4}{3}\mu(x) + \kappa(x)]u'(x) - [\tfrac{4}{3}\alpha_3(x) \\ &\quad -\alpha_1(x)]\rho''(x) + [\tfrac{2}{3}\alpha_4(x) + \alpha_2(x)]T''(x)\,, \end{aligned} \tag{9}$$

$$q(x) = -\lambda(x)T'(x) + [\tfrac{2}{3}\beta_1(x) - \beta_2(x)]u''(x)\,, \tag{10}$$

where the primes denote spatial derivatives. The transport coefficients μ (shear viscosity), κ (bulk viscosity), λ (thermal conductivity), α_i and β_i depend on space through their dependence on the local density $\rho(x)$ and temperature $T(x)$. This dependence

can be obtained from the Chapman-Enskog method [13] applied to the Enskog equation. On the other hand, the expressions for the fluxes in the NS order are derived by dropping the terms containing u'' and T''. The explicit expressions for the NS transport coefficients are

$$\kappa = \frac{4}{9}\left(\frac{\rho}{m}\right)^2 \sigma^4 \chi(\eta)(\pi m k_B T)^{1/2}, \tag{11}$$

$$\mu = \frac{1}{\chi(\eta)}[1 + \tfrac{8}{5}\eta\chi(\eta)]^2 \mu_B + \tfrac{3}{5}\kappa, \tag{12}$$

$$\lambda = \frac{1}{\chi(\eta)}[1 + \tfrac{12}{5}\eta\chi(\eta)]^2 \lambda_B + \frac{3}{2}\frac{k_B}{m}\kappa. \tag{13}$$

Here, μ_B and λ_B are the shear viscosity and the thermal conductivity of a dilute hard-sphere gas, respectively. Their values are [13]

$$\mu_B = 1.0160 \times \frac{5}{16}\left(\frac{m k_B T}{\pi}\right)^{1/2} \sigma^{-2}, \tag{14}$$

$$\lambda_B = 1.0251 \times \frac{15}{4}\frac{k_B}{m}\mu_B. \tag{15}$$

The linear Burnett coefficients given by the standard Enskog theory (SET) and the revised Enskog theory (RET) can be found in Refs. [17] and [18], respectively. For the sake of self-consistency, we write their corresponding expressions in Appendix A.

Unfortunately, the nonlinear Burnett coefficients of the Enskog equation have not been derived, although these coefficients are the same in both the SET and the RET. A possible way to overcome such difficulty is to consider the low-density gas. In this case, the complete Burnett transport coefficients are quoted for instance, in the textbook of Chapman and Cowling [13]. In the geometry of the wave, the expressions of the momentum and heat fluxes are

$$\begin{aligned} P_{xx} &= p - \tfrac{4}{3}\mu_B u' + \frac{\mu_B^2}{c^2 p}[\tfrac{2}{3}\omega_1 - \tfrac{14}{9}\omega_2 + \tfrac{2}{9}\omega_6]u'^2 \\ &\quad + \tfrac{2}{3}\frac{\mu_B^2}{c^2 \rho T}\left[\omega_2\left(\frac{u'T'}{u} - \frac{Tu'^2}{u^2} - T'' + \frac{Tu''}{u}\right)\right. \\ &\quad \left. + \omega_3 T'' + \omega_4\left(\frac{T'^2}{T} - \frac{T'u'}{u}\right) + \omega_5\frac{T'^2}{T}\right], \end{aligned} \tag{16}$$

$$\begin{aligned} q &= -\lambda_B T' + \frac{\mu_B^2}{c^2 \rho T}\left[(\theta_1 - \tfrac{8}{3}\theta_2 + 2\theta_5)u'T'\right. \\ &\quad \left. + \tfrac{2}{3}(\theta_4 - \theta_2)Tu'' + \tfrac{2}{3}\theta_3 u'\left(T' - \frac{Tu'}{u}\right)\right], \end{aligned} \tag{17}$$

where $c = 1.0160$ and the numerical values of the coefficients ω_i and θ_i are: $\omega_1 = 1.014 \times 4$, $\omega_2 = 1.014 \times 2$, $\omega_3 = 0.806 \times 3$, $\omega_4 = 0.681$, $\omega_5 = \frac{3}{2} \times 0.806$, $\omega_6 = 0.928 \times 8$, $\theta_1 = \frac{45}{4} \times 1.035$, $\theta_2 = \frac{45}{8} \times 1.035$, $\theta_3 = -3 \times 1.03$, $\theta_4 = 3 \times 0.806$ and $\theta_5 = 8.3855$. By substituting Eqs. (9) and (10) [or (16) and (17) in the case of a dilute gas] into the conservation equations (1)-(3) and using the jump conditions (4)-(6), one derives a closed system of nonlinear differential equations for $\rho(x)$, $u(x)$ and $T(x)$. Its solution must be carried out numerically. In addition, since the mathematical stability of the set of equations is directional, the numerical integration must start at the hot equilibrium side. More technical details on the integration of this system of equations can be found in Ref. [19].

3 THEORY OF HOLIAN FOR A DENSE HARD-SPHERE FLUID

The numerical difficulties inherent to the integration of the nonlinear Burnett equations have motivated the search for simpler alternatives that exhibit a better accuracy than that of the NS approximation. A possibility is to assume the validity of the linear relationships between fluxes and gradients but modifying the thermal dependence of the transport coefficients. Having in mind these requirements, Holian [7, 14] proposed a very simple and accurate theory for strong shock waves in a dilute gas. The basic idea is to use the NS equations but replacing T by T_{xx} in the expressions of the transport coefficients. Here, T_{xx} is the component of the temperature in the direction of the shock wave propagation. Very recently, Holian's recipe has been extended to a dense hard-sphere fluid [22]. In the case of a dense gas, the component of the temperature T_{xx} is, by definition, $T_{xx} = (m/\rho k_B)P_{xx}^k$, where P_{xx}^k refers to the *kinetic* part of the xx normal component of the pressure tensor. In fact, the (total) pressure tensor P can be written as $\mathsf{P} = \mathsf{P}^k + \mathsf{P}^c$, with P^c indicating the collisional transfer contribution. In order to implement the Holian's conjecture is necessary to specify T_{xx} in terms of the hydrodynamic fields ρ, u and T. This will be done below.

First, taking into account the Rankine-Hugoniot condition (5), the hydrodynamic equation (2) for the conservation of momentum can be written as

$$P_{xx}(x) + \rho(x)u^2(x) = p_0 + \rho_0 u_0^2. \tag{18}$$

On the other hand, at the NS level, the kinetic part P_{xx}^k is given by

$$P_{xx}^k(x) = \frac{\rho(x) k_B T(x)}{m} - \tfrac{4}{3}\mu^k(x) u'(x) , \qquad (19)$$

where the coefficient μ^k corresponds to the kinetic contribution to the shear viscosity μ, and its value is given by the relation [13]

$$\mu^k = \frac{1}{\chi(\eta)}[1 + \tfrac{8}{5}\eta\chi(\eta)]\mu_B . \qquad (20)$$

In the context of the Enskog equation, it must be pointed that all the NS transport coefficients are proportional to $\sqrt{T}$, i.e., $\{\mu(\rho,T), \kappa(\rho,T), \lambda(\rho,T), \mu^k(\rho,T)\} \equiv \{\tilde{\mu}(\rho), \tilde{\kappa}(\rho), \tilde{\lambda}(\rho), \tilde{\mu}^k(\rho)\}\ \sqrt{T}$. Consequently, according to the NS approximation [see Eqs. (9) and (19)], one gets

$$\frac{P_{xx}^k - \rho k_B T/m}{P_{xx} - p} = \frac{\tilde{\mu}^k}{\tilde{\mu} + \frac{3}{4}\tilde{\kappa}} \equiv A(\rho) . \qquad (21)$$

From the identities (18) and (21), one easily writes T_{xx} as a function of the hydrodynamic fields:

$$T_{xx} = T\{1 - [1 + 4\eta\chi(\eta)]A(\rho)\} + A(\rho)u\{\frac{T_0}{u_0} \times [1 + 4\eta_0\chi(\eta_0)] + \frac{m}{k_B}(u_0 - u)\} , \qquad (22)$$

where η_0 is the value of the packing fraction corresponding to the unshocked equilibrium state. In the low-density limit ($\eta \to 0$), the expression (22) reduces to the one originally obtained in previous works [7].

As said before, Holian's recipe consists in describing the shock wave profiles by means of the NS equations but setting T_{xx} instead of T in the transport coefficients expressions. Specifically, the generalization of the Holian's recipe to the case of a dense hard-sphere fluid described by the Enskog equation consists in replacing the temperature T by the value T_{xx} given by (22) into the formulas (11)-(13).

4 MONTE CARLO SIMULATION OF THE ENSKOG EQUATION

In the early 1960's, Bird [12] devised the so-called direct simulation Monte Carlo (DSMC) method to numerically solve the Boltzmann equation. This method has been widely applied to different phenomena in rarefied gases, and several comparisons with known exact solutions of the Boltzmann equation show the accuracy of the DSMC method. In the context of a dense hard-sphere fluid described by the Enskog equation, an extension of the DSMC method [the so-called Enskog simulation Monte Carlo (ESMC) method] has been recently proposed [20]. In the same way as the original DSMC, the ESMC algorithm has been shown to be a fruitful and efficient tool to solve the Enskog equation. In particular, this method reproduces quite well the density dependence of the Enskog transport coefficients, namely, the shear viscosity [20, 24], the viscometric functions [24] and the thermal conductivity [25]. Hence, the results obtained by means of the ESMC method are the adequate reference to check the performance of the different continuum approaches in describing the shock profiles.

The ESMC algorithm as applied to the plane shock wave problem proceeds as follows [21]. A system of length D along the x direction is occupied by N particles. The boundaries of the system are sufficiently far away from the shock front, so they can be considered at equilibrium. This implies that D must be much larger than the shock thickness. The system is split into L layers of width $\Delta x = D/L$ smaller than both the mean free path and the shock thickness, which is the characteristic hydrodynamic length. The number N has a statistical meaning, so that the physical density of the layer $I = 1, \ldots, L$ is $n_I = \overline{n}L(N_I/N)$, where $\overline{n}$ is the average density and N_I is the number of simulated particles in layer I. Those particles lying in cells separated from the boundaries a distance smaller than or equal to σ represent "bath" particles, while the remaining ones represent "actual" particles. The velocity distributions of the bath particles are kept to be Maxwellians. The role of these particles is to sample the upstream and downstream equilibrium conditions. The positions and velocities of all particles are updated due to free streaming and collisions. Both stages are decoupled for a time step Δt much smaller than both the mean free time and the hydrodynamic time. In the free streaming stage, the particles move freely and those particles leaving the system are reentered through the opposite boundary with the same velocity. As a consequence, the flux of mass is conserved. Before proceeding to the collision stage, the velocities of the bath particles are replaced by those randomly obtained from a Maxwellian distri-

bution of probability characterized by the upstream or downstream hydrodynamic fields, namely, $u_{0,1}$ and $T_{0,1}$.

In the ESMC method, the collision stage is modified with respect to the DSMC algorithm by incorporating the density effects present in the Enskog equation. For each layer I, a sample of $\frac{1}{2}N_I\omega_{\max}$ particles are chosen at random with equiprobability, where $\omega_{\max}$ is an upper bound of the quantity ω_{ij} defined below. For each particle i of this sample the following steps are taken: (1) a given direction $\hat{\boldsymbol{\sigma}}$ is chosen at random with equiprobability; (2) a particle j belonging to the layer J that contains the point $x_i + \sigma\hat{\sigma}_{ix}$ is chosen at random with equiprobability; (3) the collision between particles i and j is accepted with a probability equal to $\Theta(\hat{\boldsymbol{\sigma}}_i\cdot\mathbf{g}_{ij})\omega_{ij}/\omega_{\max}$, where $\mathbf{g}_{ij}\equiv\mathbf{v}_i-\mathbf{v}_j$ and $\omega_{ij}\equiv\sigma^2 4\pi(\hat{\boldsymbol{\sigma}}_i\cdot\mathbf{g}_{ij})\chi_{ij}n_J\Delta t$, χ_{ij} being the pair correlation associated with the positions of the spheres i and j; and (4) if the collision is accepted, the postcollision velocities $\mathbf{v}_i' = \mathbf{v}_i-(\hat{\boldsymbol{\sigma}}_i\cdot\mathbf{g}_{ij})\hat{\boldsymbol{\sigma}}_i$ and $\mathbf{v}_j' = \mathbf{v}_j + (\hat{\boldsymbol{\sigma}}_i\cdot\mathbf{g}_{ij})\hat{\boldsymbol{\sigma}}_i$ are *immediately* assigned to particles i and j, respectively. This change does not apply for the bath particles. In our simulations we have implemented the SET rather than the RET. This implies that $\chi_{ij} = \chi(\eta_K)$, where K denotes the layer equidistant from layers I and J. In order to avoid any systematic bias, the sorting of the cell I is chosen randomly. The initial conditions have been taken as corresponding to two different equilibrium distributions for $x < 0$ and $x > 0$ characterized by the upstream and downstream hydrodynamic fields, respectively. After a certain transient regime, the stationary state is reached. This can be tested by checking that the balance equations (1)–(3) are verified along the whole system. In the stationary state, the physical properties are evaluated in every layer by averaging over the particles inside that layer and also over an ensemble of $\mathcal{N}$ independent realizations. In each realization, the local flow velocity and temperature are, respectively, $\mathbf{u}_I = 1/N_I\sum_{i\in I}\mathbf{v}_i$ and $T_I = m/(3k_BN_I)\sum_{i\in I}(\mathbf{v}_i-\mathbf{u}_I)^2$. Once the hydrodynamic fields are measured, the dissipative fluxes $P_{xx}(x)$ and $q(x)$ can be obtained from the balance equations (1)–(3).

The quantities D, N, Δx, and Δt are technical parameters whose values must be determined depending on the case considered. In fact, the values of Δx and Δt must be chosen smaller as the shock front becomes sharper. For example, in the case of $\eta_0 = 0.2$ and $M = 1.3$ we have taken $D = 70\lambda_0$, $N = 350\,000$, $\Delta x = 0.1\lambda_0$, and $\Delta t = 0.003\lambda_0/\sqrt{2k_BT_0/m}$, λ_0 being the mean free path $\lambda_0 = [\sqrt{2}\pi\rho_0\chi(\eta_0)\sigma^2/m]^{-1}$ of the hard-sphere gas in the cold region. On the other hand, the value of $\mathcal{N}$ is typically around 5.

5 RESULTS

In previous sections we have presented the different alternatives to analyze the shock wave problem in the case of a dense hard-sphere fluid described by the Enskog equation. Now, we are in a position to check the performance of the different continuum approaches by comparison with computer simulations. In what follows, we will scale the distance x with the mean free path λ_0 of the hard-sphere dense gas in the cold region. As usual, we choose the origin $x = 0$ of the shock front as the point where $u = (u_0+u_1)/2$. An elemental dimensional analysis allows us to conclude that the relevant dimensionless parameters characterizing the problem can be taken as the packing fraction upstream, η_0, and the Mach number $M \equiv u_0/a_0$, where a_0 is the speed of sound upstream. By using thermodynamics relations [26], it can be shown that the speed of sound a in a hard-sphere fluid is

$$a = \left(\frac{5k_BT}{3m}\right)^{1/2}\left[1+8\eta\chi+\tfrac{4}{5}\eta^2\left(8\chi^2+3\frac{d\chi}{d\eta}\right)\right]^{1/2}. \tag{23}$$

Note that, in contrast to other choices, both λ_0 and a_0 refer to quantities of a *dense* gas, so that M is the real Mach number.

In Fig. 1 we display the (reduced) velocity and temperature profiles as obtained from the NS equations and the ESMC simulations for $\eta_0 = 0.2$ and $M = 1.3$. Since the value of the Mach number is not large enough, the NS approximation describes the shock profiles accurately, so that no further approximation is needed. On the other hand, we have also compared our Monte Carlo data with those obtained from molecular dynamics simulations [27], finding an excellent agreement. This last result confirms the validity of the SET to describe the shock wave profiles for moderate densities.

Discrepancies between the NS profiles and the simulation results appear as the shock front becomes sharper (namely, η_0 decreases and/or M increases). As an illustration, Figure 2 shows the velocity and temperature profiles for $\eta_0 = 0.2$ and $M = 3.5$ as ob-

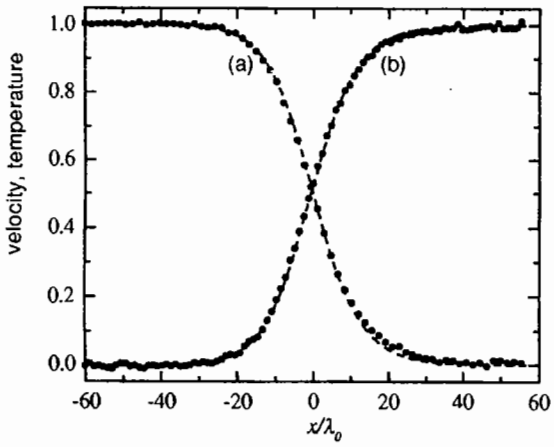

Figure 1: Profiles of (a) the reduced velocity $(u - u_1)/(u_0 - u_1)$ and (b) the reduced temperature $(T - T_0)/(T_1 - T_0)$ at $\eta_0 = 0.2$ and $M = 1.3$. The dashed lines correspond to the NS solutions, and the circles refer to the ESMC data.

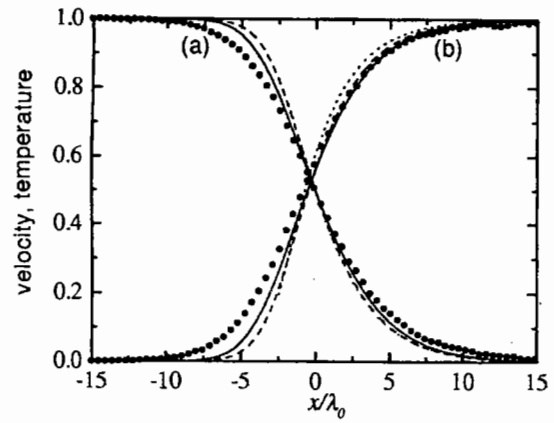

Figure 2: Profiles of (a) the reduced velocity $(u - u_1)/(u_0 - u_1)$ and (b) the reduced temperature $(T - T_0)/(T_1 - T_0)$ at $\eta_0 = 0.2$ and $M = 3.5$. The solid lines correspond to the Holian theory, the dashed lines to the NS theory, and the dotted lines refer to the (linear) Burnett theory. The circles are the ESMC data.

tained from the different continuum approaches and the ESMC simulation method. We have calculated the (linear) Burnett profiles by considering the transport coefficients given by the SET and the RET, but they are practically indistinguishable. Due to numerical instabilities, these profiles are interrupted on the cold side [19]. Fiscko and Chapman [2] were able to overcome this difficulty in the case of a dilute gas by solving the time-dependent equations rather than the steady-state ones. For our purposes, this does not represent a serious drawback. In fact, we will focus later on the shock thickness which is evaluated from the maximum value of the density gradient. For the values of η_0 and M considered, the density profile near its inflection point is not affected by the numerical instabilities. The results indicate that the velocity and temperature profiles are rather well described by the NS and Holian theories on the hot side. Nevertheless, it must be pointed out that the theoretical curves fail to capture the longer relaxation towards the cold end equilibrium values reflected in the simulation results. In any case, the superiority of the Holian approach is clear. In Fig. 3 we show the stress

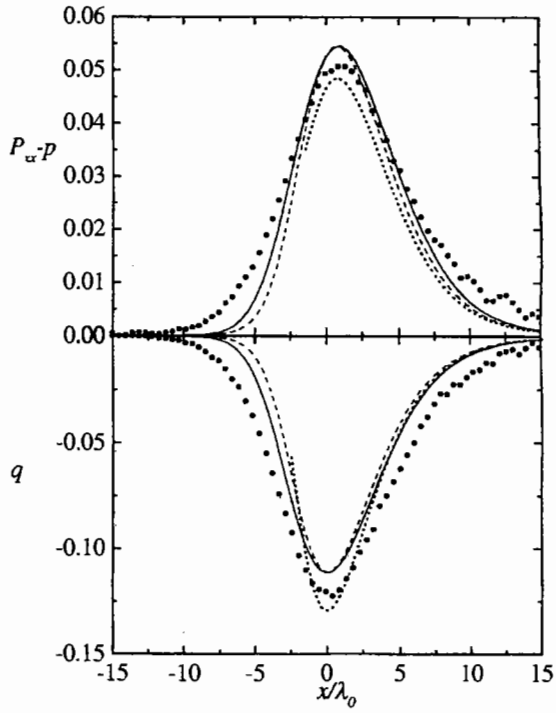

Figure 3: The same as in Fig. 2, but for the stress $P_{xx} - p$, measured in units of $2k_BT/\lambda_0^3$, and for the heat flux q, measured in units of $m(2k_BT_0/m)^{3/2}/\lambda_0^3$.

$P_{xx} - p$ and the heat flux q profiles for the same values of the packing fraction η_0 and Mach number M. The agreement is worse for these quantities, but the Holian theory improves again the predictions made by the remaining continuum approaches.

In order to carried out a more systematic study, it is convenient to introduce a parameter that captures the global shape of the shock wave profiles. Since the velocity and temperature profiles exhibit in this problem a high degree of symmetry, a good candidate to asses the merit of the different theories is the shock thickness. As usual, we define the reciprocal shock thickness as the maximum of the normalized density gradient:

$$\delta^{-1} = \frac{1}{\rho_1 - \rho_0} \left(\frac{d\rho}{dx} \right)_{\max} . \tag{24}$$

In Fig. 4 we display the density dependence of δ^{-1} at $M = 2$. The error bars on the simulation points indicate the uncertainty associated with statistical fluctuations and with the localization of $(d\rho/dx)_{\max}$. In general, all the theories correctly predict that the shock thickness (in units of the upstream mean free path λ_0) increases with density, but underestimate its value. In the low-density regime it is clear that the (linear) Burnett theory leads to a better agreement with simulations than both the NS and Holian predictions. However, as the density increases the Holian theory becomes superior to the Burnett one. In fact, for $\eta_0 \simeq 0.1$ (and $M = 2$) both approaches lead to the same value of δ. Beyond this density boundary value, the Holian theory is clearly the best overall performance. According to the different simulations carried out for a range of densities and Mach numbers, we can conclude that the density value beyond which the Holian theory improves the Burnett predictions is practically independent of the Mach number considered. From a practical point of view, we can state that for $M \gtrsim 1.5$, only if $\eta_0 \lesssim 0.1$, the (linear) Burnett theory provides the best description. Outside this density range, the Holian theory is clearly superior to all other continuum approaches.

As a complement, in Fig. 5 we show the dependence of δ on M for two values of the density. In the low density regime ($\eta_0 = 0$) we see again that the Burnett theory leads to a better agreement with simulations than both the NS and Holian predictions. A similar conclusion was also reached in Ref. [15]. Nevertheless, it must be pointed out that the best overall performance is given by the *linearized* rather than the *complete* [see Eqs. (16) and (17)] Burnett equations. In fact, for $\eta_0 = 0$ and $M = 134$ (which is the case studied in Refs. [6], [14], and [15]), we

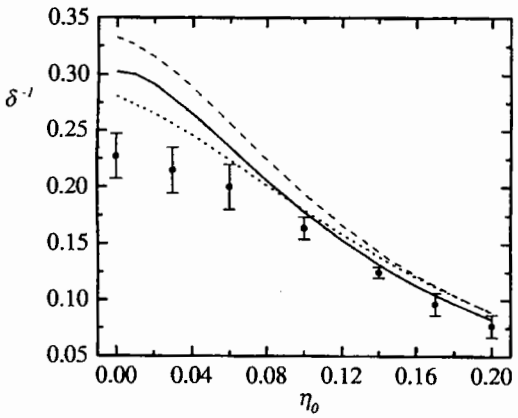

Figure 4: Density dependence of the reciprocal shock thickness (in units of the mean free path λ_0) at $M = 2$ The solid line corresponds to the Holian theory, the dashed line to the NS theory, and the dotted line refers to the (linear) Burnett theory. The circles are the ESMC data.

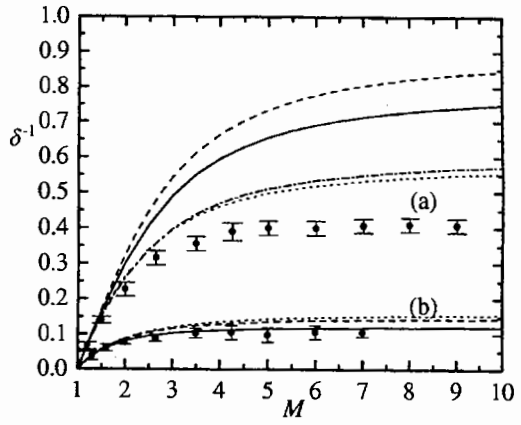

Figure 5: Mach dependence of the reciprocal shock thickness (in units of the mean free path λ_0) at (a) $\eta_0 = 0$ and (b) $\eta_0 = 0.2$ as obtained from the Holian theory (—), the NS theory (-- — —), the linear Burnett theory (- - -), and the full Burnett theory (— - — -) . The circles are the ESMC data.

get $\delta^{\rm NS} = 1.13\lambda_0$ for the NS theory, $\delta^{\rm H} = 1.27\lambda_0$ for the Holian theory, $\delta^{\rm B} = 1.68\lambda_0$ for the complete Burnett theory, and $\delta^{\rm LB} = 1.74\lambda_0$ for the linear Burnett theory, while the thickness estimated from the molecular dynamics results of Ref. [6] is $\delta = 2.3\lambda_0$. Taking into account these results, one has serious doubts about the convenience of retaining super-Burnett and higher order gradient terms as the Mach number increases.

On the other hand, for the finite density $\eta_0 = 0.2$, surprisingly, the Burnett thickness is smaller than the NS thickness for sufficiently large value of the Mach number M. Considering the previous discussion about the results obtained for a dilute gas, one could suggest that the above discrepancy is not only due to the absence of the nonlinear Burnett terms in the constitutive equations but also to the nonconvergent asymptotic character of the Chapman-Enskog expansion. Moreover, the NS predictions are *clearly* improved when Holian's recipe is introduced. In fact, when the error bars are accounted for, all the simulation results fall on top of the theoretical Holian line. Thus, for $\eta_0 = 0.2$ and $M = 3.5$ one gets $\delta^{\rm NS} = 8.09\lambda_0$, $\delta^{\rm LB} = 7.76\lambda_0$, and $\delta^{\rm H} = 9.27\lambda_0$, while the simulation result is $\delta = (10 \pm 1)\lambda_0$.

6 CONCLUDING REMARKS

In this paper we have offered an overview of recent work on plane shock waves in a hard-sphere fluid within the framework of the Enskog theory. The results have been obtained from three different and complementary routes: (i) the standard hydrodynamic approaches at the levels of NS and (linear) Burnett orders; (ii) the use of Holian's conjecture; and (iii) the numerical solution of the full Enskog equation by means of the ESMC method. The comparison with simulation results allows us to assess the merit of the different approaches. At a qualitatively level, we can conclude that the theoretical predictions underestimate the shock thickness. This effect becomes more important at low densities and high Mach numbers. In other words, the hydrodynamic theories tend to provide a better description of the shock-wave structure as the density increases. This can be partially explained by the fact that the thickness, in units of the mean free path, increases with the density. On the other hand, for finite densities the Holian theory agrees much better with Monte Carlo simulations than the NS and (linear) Burnett approximations, in contrast to the well-known superiority of the (linear) Burnett theory for dilute gases. In addition, the Holian's recipe combines reasonable accuracy for such a complicated problem with relative simplicity, since it only takes into account the linear relationships between fluxes and gradients. In this sense, it must be noticed that, although the Holian constitutive equations are *formally* linear, a non-Newtonian description is carried out due to the *nonlinear* dependence of the viscosity and thermal conductivity coefficients on the strain rate a'.

Finally, we must point out that since the present results have been derived in the context of the Enskog equation, the above conclusions cannot be extrapolated without caution to real systems. In particular, one would hope that the Holian's recipe would work not only for dense hard-sphere gases but for other fluids. However, this extension is not clearcut. In this context, the performance of more simulations would be welcome to show if the above conjecture whether fulfilled.

Partial support from the DGES (Spain) through Grant No. PB97-1501 and from the Junta de Extremadura (Fondo Social Europeo) through Grant No. IPR99C031 is acknowledged.

A LINEAR BURNETT TRANSPORT COEFFICIENTS FOR A DENSE HARD-SPHERE FLUID

The linear Burnett transport coefficients can be written as $\alpha_1 = (\mu_B/c\rho)^2 g_{\alpha_1}$, $\alpha_2 = (\mu_B^2/c^2\rho T) g_{\alpha_2}$, $\alpha_3 = (\mu_B/c\rho)^2 g_{\alpha_3}$, $\alpha_4 = (\mu_B^2/c^2\rho T) g_{\alpha_4}$, $\beta_1 = (\mu_B^2/c^2\rho) g_{\beta_1}$ and $\beta_2 = (\mu_B^2/c^2\rho) g_{\beta_2}$, where $c = 1.0160$ and the functions g_{α_i} and g_{β_i} are dimensionless quantities. In the particular case of a hard-sphere fluid described by the SET, these functions are given by the following expressions [17]:

$$g_{\alpha_1}(\eta) = \frac{4096}{25\pi}\frac{1}{\chi^2}\left(1 + \frac{1}{8}\frac{\eta}{\chi}\frac{\partial\chi}{\partial\eta}\right)(\chi\eta)^3 , \tag{25}$$

$$g_{\alpha_2}(\eta) = \frac{96}{5\pi}\frac{1}{\chi^2}\left(1 + \frac{20}{3}\chi\eta\right)(\chi\eta)^2 , \tag{26}$$

$$g_{\alpha_3}(\eta) = \frac{1}{\chi^2}\left\{1+\tfrac{56}{5}\chi\eta+\tfrac{704}{25}(\chi\eta)^2 + \left(\tfrac{512}{25}-\tfrac{12\,288}{125\pi}\right)(\chi\eta)^3+\left[4+\tfrac{64}{5}\chi\eta + \left(\tfrac{256}{25}-\tfrac{1536}{125\pi}\right)(\chi\eta)^2\right]\frac{\partial\chi}{\partial\eta}\eta^2\right\}, \quad (27)$$

$$g_{\alpha_4}(\eta) = \frac{1}{\chi^2}\left[1+\tfrac{24}{5}\chi\eta+\left(\tfrac{48}{5}+\tfrac{2112}{25\pi}\right)(\chi\eta)^2 + \left(\tfrac{896}{125}+\tfrac{31\,488}{125\pi}\right)(\chi\eta)^3\right], \quad (28)$$

$$g_{\beta_1}(\eta) = 3\frac{1}{\chi^2}\left[1+\tfrac{32}{5}\chi\eta+\left(\tfrac{336}{25}+\tfrac{704}{25\pi}\right)(\chi\eta)^2 + \left(\tfrac{1152}{125}+\tfrac{7936}{125\pi}\right)(\chi\eta)^3\right], \quad (29)$$

$$g_{\beta_2}(\eta) = \tfrac{15}{4}\frac{1}{\chi^2}\left[1+\tfrac{44}{5}\chi\eta+\left(\tfrac{624}{25}-\tfrac{128}{25\pi}\right)(\chi\eta)^2 + \left(\tfrac{576}{25}-\tfrac{512}{25\pi}\right)(\chi\eta)^3\right]. \quad (30)$$

The same formulas hold for the RET except for g_{α_1} and g_{α_3} which are given by [18]

$$g_{\alpha_1}(\eta) = \tfrac{4096}{25\pi}\frac{1}{\chi^2}\left(1-\tfrac{37}{40}\frac{\eta}{\chi}\frac{\partial\chi}{\partial\eta}\right)(\chi\eta)^3, \quad (31)$$

$$g_{\alpha_3}(\eta) = \frac{1}{\chi^2}\left\{1+\tfrac{56}{5}\chi\eta+\tfrac{704}{25}(\chi\eta)^2 + \left(\tfrac{512}{25}-\tfrac{12\,288}{125\pi}\right)(\chi\eta)^3+\left[4+\tfrac{64}{5}\chi\eta + \left(\tfrac{256}{25}+\tfrac{3264}{125\pi}\right)(\chi\eta)^2\right]\frac{\partial\chi}{\partial\eta}\eta^2\right\}. \quad (32)$$

REFERENCES

[1] Hirschfelder, J. O., Curtis, C. F. & Bird R. B. 1954. Molecular Theory of Gases and Liquids, Wiley, New York.

[2] Fiscko, K. A. & Chapman, D. R. 1989. In: Muntz, E P., Weaver, D. P. & Campbell, D. H. (Editors), Rarefied Gas Dynamics, Page 374, AIAA, Washington.

[3] Liepmann, H. W., Narashima, R. & Chaine, M. T. 1962. Phys. Fluids 5, 1313.

[4] Lumpkin III, F. E. & Chapman, D. R. 1992. J. Thermophys. Heat Transfer 6, 419.

[5] Zhong, X., MacCormack, R. W. & Chapman, D. R. 1993. AIAA J. 31, 1036.

[6] Salomons, E. & Mareschal, M. 1992. Phys. Rev. Lett. 69, 269.

[7] Holian, B. L. 1988. Phys. Rev. A 37, 2562.

[8] Mott-Smith, H. M. 1951. Phys. Rev. 82, 885.

[9] Grad, H. 1952. Comuum. Pure Appl. Math. 5, 257; Holway, L. H. 1964. Phys. Fluids 7, 911; Weiss, W. 1995. Phys. Rev. E 52, R5760; 1996. Phys. Fluids 8, 1689.

[10] Hoover, W. G. 1979. Phys. Rev. Lett. 42, 1531.

[11] Holian, B. L., Hoover, W. G., Moran B. & Straub, G. K., 1980. Phys. Rev. A 22, 2798.

[12] Bird, G. A. 1994. Molecular Gas Dynamics and the Direct Simulation of Gas Flows, Clarendon, Oxford.

[13] Chapman, S. & Cowling, T. G. 1970. The Mathematical Theory of Nonuniform Gases, Cambridge University Press, Cambridge; Ferziger, J. & Kaper, H. 1972. Mathematical Theory of Transport Processes in Gases, North-Holland, Amsterdam.

[14] Holian, B. L., Patterson, C. W., Mareschal M. & Salomons, E. 1993. Phys. Rev. E 47, R24.

[15] Uribe, F., Velasco, R. M & García-Colín. 1998. Phys. Rev. Lett. 81, 2044.

[16] van Beijeren, H. & Ernst, M. 1973. Phys. Lett. A 43, 637; 1973. Physica A 68, 437.

[17] Alves, S. R. & Kremer, G. M. 1990. Physica A 164, 759

[18] López de Haro, M. & Garzó, V. 1993. Physica A 197, 98.

[19] López de Haro, M. & Garzó, V. 1995. Phys. Rev. E 52, 5688.

[20] Montanero, J. M. & Santos, A. 1996. Phys. Rev. E 54, 438; 1997. Phys. Fluids 9, 2057.

[21] Montanero, J. M., López de Haro, M., Garzó, V. & Santos, A. 1998. Phys. Rev. E 58, 7319.

[22] Montanero, J. M., López de Haro, M., Santos, A. & Garzó, V. 1999. Phys. Rev. E 60, 7592.

[23] Carnahan, N. F. & Starling, K. E. 1969. J. Chem. Phys. 51, 635.

[24] Montanero, J. M. & Santos, A. 1997. Physica A 240, 229.

[25] Montanero, J. M. & Santos, A. 1998. In: Shen, C. (Editor), 20th International Symposium on Rarefied Gas Dynamics, Page 113, Peking University Press, Beijing.

[26] Callen, H. B. 1959. Thermodynamics, Wiley, New York.

[27] Frezzotti, A. 1998. Comput. Math. Appl. 35, 103.